Design and Optimization of an Index Finger Exoskeleton With Semi-Wrapped Fixtures and Series Elastic Actuators

Ning Sun, Long Cheng, *Senior Member, IEEE*, Xiuze Xia, and Lijun Han

***Abstract*— This paper proposes a novel index finger exoskeleton with semi-wrapped fixtures and elastomer-based clutched series elastic actuators. The semi-wrapped fixture is similar to a clip, which improves the convenience of donning/doffing and connection stability. The elastomer-based clutched series elastic actuator can limit the maximum transmission torque and improve passive safety. Second, the kinematic compatibility of the exoskeleton mechanism for the proximal interphalangeal joint is analyzed, and its kineto-statics model is built. To avoid the damage caused by the force along the phalanx, considering the individual difference in the size of the finger segment, a two-level optimization method is proposed to minimize the force along the phalanx. Finally, the performance of the proposed index finger exoskeleton is tested. Statistical results indicate that the donning/doffing time of the semi-wrapped fixture is significantly less than that of the Velcro. Compared with the Velcro, the average value of the maximum relative displacement between the fixture and the phalanx is reduced by 59.7%. Compared with the exoskeleton before optimization, the maximum force along the phalanx generated by the exoskeleton after optimization is reduced by 23.65%. The experimental results show that the proposed index finger exoskeleton can improve the convenience of donning/doffing, connection stability, comfort, and passive safety.**

***Index Terms*— Finger exoskeleton, semi-wrapped fixture, series elastic actuator, two-level optimization method.**

I. Introduction

THE hand plays a fundamental role in the performance of daily activities, such as communication through gestures and typing, transporting objects, and manipulating tools. However, stroke, spinal cord injury, and occupational accidents often lead to the loss of hand motor function [1], [2]. To rebuild the patient's hand motor function, hand exoskeletal robots were proposed to assist patients in rehabilitation training, such as moving objects [3] and repetitive simple grasp-release exercises [4].

Hand exoskeletal robots can be divided into soft exoskeletons and rigid linkage-type exoskeletons [5]. Soft exoskeletons are made of deformable materials [6], [7], which have the advantages of comfort, low obtrusiveness, lightness, portability, and user-friendliness [8]. They adopt a jointless structure that can conform to the shape of the user's finger. The disadvantages of these exoskeletons are their limited force/torque output, independent driving joints, and sensing and control capabilities [9]. Compared with soft exoskeletons, rigid linkage-type exoskeletons are manufactured with high rigidity material, which can provide sufficient force/torque, achieve accurate control, and independently control joint movement. However, these exoskeletons have a large weight and encumbrance, as well as the problem of human-exoskeleton axis misalignment. Human-exoskeleton axis misalignment can cause undesired interaction forces, which can lead to discomfort and even injury.

To achieve human-exoskeleton axis self-alignment, researchers have proposed various rigid linkage-type exoskeletons, such as joint direct alignment [10], [11], planar self-alignment [12], [13], [14], and spatial self-alignment [15]. In our previous study, a spatial self-aligning index finger exoskeleton was proposed to realize flexion/extension (f/e) and adduction/abduction (a/a) motions [16]. However, the previously proposed index finger exoskeleton generates a force along the middle phalanx since an R pair is used between the proximal interphalangeal joint (PIP) exoskeleton and the middle phalanx. The force along the phalanx loads the joint without resulting in any joint movement and increases the related risk of skin tissue damage. Therefore, how to reduce the force along the phalanx requires further research.

The design of the fixture between the exoskeleton and the finger segment is another challenging task for rigid linkage-type exoskeletons. The fixture is directly attached or donned on the hand. It is not only the physical contact interface between the wearer and the exoskeleton but also an important channel for information transmissions such as motion and force feedback. Therefore, a good fixture is one of the important factors to improve the performance of the hand exoskeletal robot. The

Manuscript received 10 August 2022; revised 7 January 2023 and 28 April 2023; accepted 28 May 2023. Date of publication 6 June 2023; date of current version 13 June 2023. This work was supported in part by the National Natural Science Foundation of China under Grant 62025307 and Grant U1913209. *(Corresponding author: Long Cheng.)*

This work involved human subjects or animals in its research. Approval of all ethical and experimental procedures and protocols was granted by the Institute of Automation Chinese, Academy of Sciences, under Approval No. IA-202044.

The authors are with the State Key Laboratory of Multimodal Artificial Intelligence Systems, Institute of Automation, Chinese Academy of Sciences, Beijing 100190, China, and also with the School of Artificial Intelligence, University of Chinese Academy of Sciences, Beijing 100049, China (e-mail: long.cheng@ia.ac.cn).

Digital Object Identifier 10.1109/TNSRE.2023.3283407

fixtures can be divided into fully-wrapped fixtures and semi-wrapped fixtures. The fully-wrapped fixtures surround the phalanx, such as Velcro [17], [18], double ring fully-wrapped fixture [19], and ring fully-wrapped fixture [20]. These fixtures cannot provide the attaching force, resulting in a large relative displacement between the exoskeleton and the finger segment, and coverage of the finger pulp, making the finger lose the function of sensing object texture and sliding motion. Compared with the fully-wrapped fixtures, the semi-wrapped fixtures do not need to cover the finger pulp, which can keep the finger tactile and pressure sensitive. They enable users to avoid complicated and multiple donning/doffing motions, and convey a grasping force and slip motion in grasping tasks. Vertongen *et al.* designed a semi-wrapped fixture by matching the shape of the finger segments [21]. This semi-wrapping fixture needs to be customized for different users since the shape of fingers varies between individuals. Hasegawa *et al.* designed a C-type semi-wrapped fixture for a hand exoskeletal robot [22]. The fixture is composed of a C-type memory alloy, an air chamber, and an additional pneumatic drive. The additional pneumatic drive is applied to achieve donning and doffing, which increases the complexity of the system. Therefore, the semi-wrapped fixture needs further research.

In addition, force feedback and force control are essential to the physical human-exoskeleton interaction [23]. With the force controller, hand exoskeletal robots can compensate for the unwanted force and provide proper force as needed, which can exert the patients' residual ability and improve their active participation [24]. To achieve force control, researchers have applied a series elastic actuator (SEA) to a rigid linkage-type exoskeleton, such as linear compression spring SEA [25], helical torsion spring SEA [26], and structure spring SEA [27]. However, the elastic element of these SEAs can only deform within a certain range. A collision between the patient and the exoskeleton can occur due to sudden movements (their motion range beyond the deformation range of the elastic element) caused by the patients' muscle spasm, which can generate an excessive human-machine interaction force. In our previous study, an elastomer-based clutched SEA was developed to improve passive safety [28]. However, the proposed SEA has not yet been applied to hand exoskeletal robots.

In this paper, a novel index finger exoskeleton with semi-wrapped fixtures and elastomer-based clutched SEAs is proposed. The contributions of this paper can be summarized as follows: 1) An index finger exoskeleton with elastomer-based clutched SEAs is proposed, which improves its passive safety. 2) A semi-wrapped fixture is designed and applied in the index finger exoskeleton to improve the convenience of donning/doffing and connection stability. Its operation process is similar to that of the clip. 3) Considering the individual differences in the finger segment size, a two-level optimization method for the PIP exoskeleton is proposed to reduce the force along the phalanx.

The rest of this paper is organized as follows. In Section II, the index finger exoskeleton is designed and introduced. In Sections III and IV, the kinematics and kineto-statics models of the PIP exoskeleton chain are established and analyzed, and a two-level optimization method for the PIP exoskeleton chain is proposed. Section V presents the experimental setup. The experimental results are reported and discussed in Section VI. Section VII gives the conclusion.

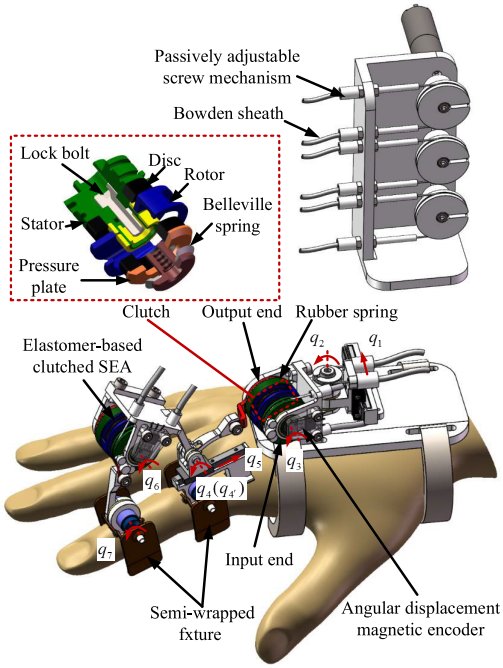

Fig. 1. Overall structure of index finger exoskeleton with the semi-wrapped fixture and the elastomer-based clutched SEA.

II. Exoskeleton Design

A. Mechanism Design

An index finger exoskeleton with semi-wrapped fixtures and elastomer-based clutched SEAs is designed, which is shown in Fig. 1. The weight of the proposed index finger exoskeleton donned on the index finger is approximately 184 g, and its maximum height (the exoskeleton above the back of the hand) is approximately 50 mm. The mechanism configuration of the index finger exoskeleton is the same as that described in ref. [16], which consists of the metacarpophalangeal joint (MCP) closed-loop kinematic chain (P3RPU) and PIP closed-loop kinematic chain (4R). The exoskeleton joint q_2 is directly driven by a Bowden-cable system. The exoskeleton joints q_3, q_6 are driven by the elastomer-based clutched SEAs proposed in ref. [28]. The elastomer-based clutched SEA is mainly composed of the input end, the output end, the rubber spring, the clutch, and the encoders. The clutch is connected in series between the input end and the rubber spring to limit the transmissible torque. The clutch is mainly composed of a lock bolt, a Belleville spring, a pressure plate, two thin disks, a rotor, and a stator. The lock bolt can deform the Belleville spring by tightening, and the Belleville spring can provide a driving force to the pressure plate. The pressure plate is used to compress two thin disks that are coupled to the rotor and the stator of the clutch. When the maximum transmission torque is reached, the rotor and stator can rotate relatively. Two angle encoders are installed at the sides of the input end and output end. When the stator and rotor of the clutch do not rotate relative to each other, the deformation of

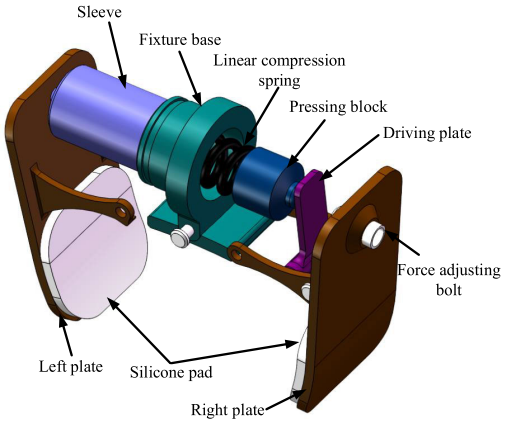

Fig. 2. Mechanical structure of the semi-wrapped fixture.

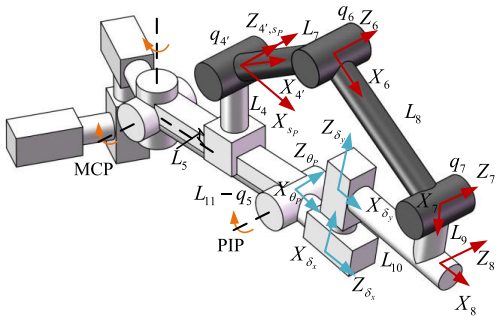

Fig. 3. Kinematics of the PIP joint and the PIP exoskeleton chain.

the rubber spring can be obtained by subtracting the positions of the input end and output end. The index finger exoskeleton is fixed with the Velcro to the dorsum of the hand. The index finger exoskeleton is connected with the proximal phalanx and the middle phalanx by the semi-wrapped fixture. The operating process of the semi-wrapped fixture is similar to that of a clip, which is convenient for patients to don and doff. In addition, the semi-wrapped fixture can provide the exoskeleton phalanx attaching force and improve the connection stability.

Remark 1: The two closed-loop kinematic chains for the MCP and PIP joints are designed to achieve the f/e and a/a motions. Similar to the index finger, other fingers are mainly composed of single revolute joints (the interphalangeal joints) and double revolute joints (the MCP joint and the carpometacarpal joint). Therefore, the mechanism configuration of the two closed-loop kinematic chains can be applied to other finger corresponding joints. For example, an untethered adaptive thumb exoskeleton based on the mechanism configuration of the proposed index finger exoskeleton was developed [29]. However, the mechanical structure of the exoskeleton should be redesigned to obtain sufficient installation space.

B. Semi-Wrapped Fixture Design

Figure 2 shows the overall structure of the semi-wrapped fixture. The semi-wrapped fixture is mainly composed of the fixture base, linear compression spring, force adjusting bolt, pressing block, etc. The left plate and right plate are installed on the fixture base through a pin shaft, and they can rotate relatively around the pin shaft. The sleeve is placed on the fixture base, which can slide relative to the fixture base. The linear compression spring is placed inside the sleeve to provide the attaching force between the exoskeleton and the phalanx. The two ends of the linear compression spring are in contact with the sleeve and the pressing block. One end of the sleeve and the pressing block away from the linear compression spring contact the left plate and the driving plate, respectively. The driving plate is installed on the right plate through a pin shaft, which can rotate relative to the right plate. The force adjusting bolt is screwed on the right plate, and its one end is in contact with the driving plate. The deformation of the linear compression spring can be changed by rotating the force adjusting bolt. It is worth noting that the linear compression spring needs to be precompressed to ensure the minimum space between the left plate and right plate. To improve the comfort of the semi-wrapped fixture, a layer of silicone pad can be attached to the part of the left/right plate in contact with the fingers.

III. Kinematics Analysis

A. Kinematic Compatibility Analysis

According to the anatomy of the hand, the PIP joint is an interphalangeal trochlear joint with one degree of freedom. It is worth noting that the axis of the PIP joint can relax during rotation because of the soft tissue in the PIP joint, that is, the position of the PIP joint axis can change with the change of joint motion angle. Human-exoskeleton joint axis misalignment can be generated due to the change of the PIP joint axis position. Here, the PIP joint's misaligning displacements are modeled as two translations in two orthogonal directions. The kinematics model of the index finger PIP joint shown in Fig. 3 consists of one orthogonal rotation and two misaligning translations. Figure 3 also shows the kinematics of the proposed PIP exoskeleton chain. The kinematic compatibility of the PIP exoskeleton chain is analyzed based on the kinematics of the PIP closed-loop kinematics chain.

As shown in Fig. 3, the coordinate systems of the PIP exoskeleton chain based on the D-H method are sequentially established and are expressed by the red arrow line. The D-H parameters of the PIP exoskeleton chain are listed in Table I. The coordinate systems of the PIP joint based on the matrix transformation method are established and are expressed by the blue arrow line. $L_{11} - q_5$ represents the distance between the rotation center of the PIP joint and the exoskeleton joint q_5 along the proximal phalanx, in which q_5 is regarded as constant in the PIP closed-loop kinematic chain. L_4, L_7, and L_8 stand for the corresponding link length. L_5 is the distance between the sliding plane of the exoskeleton joint q_5 and the central axis of the proximal phalanx. L_9 represents the distance between the exoskeleton joint q_7 and the central axis of the middle phalanx. L_{10} is the distance between the central position of the connection between the exoskeleton and the middle phalanx and the PIP joint.

Define the rotation motion of the PIP joint as θ_P, and define the misaligning displacements as $\delta_P = [\delta_x \ \delta_y]^{\mathrm{T}}$. The

TABLE I
D-H PARAMETERS OF THE PIP EXOSKELETON CHAIN

i	α_{i-1}	a_{i-1}	d_i	θ_i
4'	0	0	0	$-q_{4'}$
6	0	L_7	0	q_6
7	0	L_8	0	q_7
8	0	L_9	0	90

kinematics of the PIP closed-loop kinematic chain can be expressed as

$$ {}^{s_P}_{e_P}T^{E}(q_P) = {}^{s_P}_{e_P}T^{H}(\theta_P, \delta_P), \tag{1} $$

where $q_P = [q_{4'}\ q_6\ q_7]^{\mathrm{T}}$ is the angle variables of the PIP exoskeleton joints, s_P is a fixed global reference frame $(O_{s_P} - X_{s_P}, Y_{s_P}, Z_{s_P})$, e_P stands for the intersection coordinate system of the PIP exoskeleton chain and the PIP joint chain. ${}^{s_P}_{e_P}T^{E}(q_P)$ represents the relative position and orientation of the coordinate system e_P and the reference frame s_P of the exoskeleton chain. ${}^{s_P}_{e_P}T^{H}(\theta_P, \delta_P)$ is the relative position and orientation of the coordinate system e_P and the reference frame s_P of the PIP joint chain.

The left and right terms of Eq. (1) could be obtained by sequentially multiplying the homogeneous transformation matrices of adjacent coordinate systems along the exoskeleton chain and the PIP joint chain. Based on the D-H method, ${}^{s_P}_{e_P}T^{E}(q_P)$ can be expressed as

$$ {}^{s_P}_{e_P}T^{E}(q_P) = {}^{s_P}_{4'}T^{4'}_{6}T^{6}_{7}T^{7}_{e_P(8)}T. \tag{2} $$

where

$$ {}^{i-1}_{i}T = \begin{bmatrix} {}^{i-1}_{i}R & {}^{i-1}_{i}P \\ 0 & 1 \end{bmatrix} $$

with ${}^{i-1}_{i}R$ and ${}^{i-1}_{i}P$ representing the rotation matrix and the translation vector, respectively. Based on the matrix transformation method, ${}^{s_P}_{e_P}T^{H}(\theta_P, \delta_P)$ can be expressed as

$$ {}^{s_P}_{e_P}T^{H}(\theta_P, \delta_P) = {}^{s_P}_{\theta_P}T^{\theta_P}_{\delta_x}T^{\delta_x}_{\delta_y}T^{\delta_y}_{e_P(8)}T, \tag{3} $$

where

$$ {}^{s_P}_{\theta_P}T = \begin{bmatrix} c_{\theta_P} & -s_{\theta_P} & 0 & V \\ s_{\theta_P} & c_{\theta_P} & 0 & H \\ 0 & 0 & 1 & 0 \\ 0 & 0 & 0 & 1 \end{bmatrix}^{\theta_P}_{\delta_x} \quad T = \begin{bmatrix} 0 & 0 & 1 & \delta_x \\ -1 & 0 & 0 & 0 \\ 0 & -1 & 0 & 0 \\ 0 & 0 & 0 & 1 \end{bmatrix}, $$

$$ {}^{\delta_x}_{\delta_y}T = \begin{bmatrix} 0 & 0 & 1 & \delta_y \\ 0 & -1 & 0 & 0 \\ 1 & 0 & 0 & 0 \\ 0 & 0 & 0 & 1 \end{bmatrix}^{\delta_y}_{e_P(8)} \quad T = \begin{bmatrix} 1 & 0 & 0 & L_{10} \\ 0 & 0 & 1 & 0 \\ 0 & -1 & 0 & 0 \\ 0 & 0 & 0 & 1 \end{bmatrix}, $$

with $V = L_{11} - q_5$, $H = L_4 + L_5$, $s_{\theta_P} = \sin\theta_P$, $c_{\theta_P} = \cos\theta_P$.

Substituting the results of Eqs. (2) and (3) into Eq. (1) yields

$$ \begin{pmatrix} \theta_P \\ \delta_x \\ \delta_y \end{pmatrix} = \begin{pmatrix} q_6 - q_{4'} + q_7 - \pi/2 \\ Vc_{\theta_P} - Hs_{\theta_P} + L_7c_{67} + L_8s_7 - L_{10} \\ Vs_{\theta_P} + Hc_{\theta_P} + L_7s_{67} - L_8c_7 - L_9 \end{pmatrix}, \tag{4} $$

where $s_{67} = \sin(q_6 + q_7 - \pi/2)$, $c_{67} = \cos(q_6 + q_7 - \pi/2)$, $s_7 = \sin q_7$, $c_7 = \cos q_7$.

This result indicates that any position (θ_P, δ_x and δ_y) of the PIP joint could be achieved through the exoskeleton chain. In other words, the proposed mechanism is compatible with the kinematics of the PIP joint.

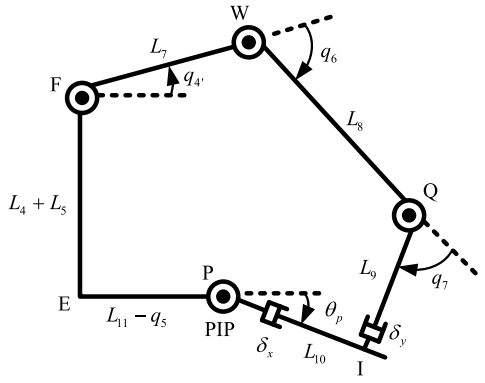

Fig. 4. Kinematics diagram of the PIP joint and the PIP exoskeleton chain.

B. Forward Kinematics

Here, the forward kinematics model of the PIP closed-loop kinematic chain is established based on the geometric method since it is difficult to simplify the display expression of the forward kinematics based on Eq. (4). Figure 4 shows the kinematic diagram of the PIP joint and the PIP exoskeleton chain. For the convenience of expression, the exoskeleton joints $q_{4'}$, q_6, q_7 and the PIP joint are named points F, W, Q and P, respectively. The intersection of the exoskeleton joint $q_{4'}$ perpendicular to the central axis of the proximal phalanx and the intersection of the exoskeleton joint q_7 perpendicular to the central axis of the middle phalanx are named points E and I, respectively.

The PIP closed-loop kinematic chain can be decomposed into two triangles: triangle FWQ and FPQ. It is worth noting that two triangles have a common edge FQ. According to the law of cosines, the length L_{FQ} of edge FQ in triangle FWQ can be expressed as

$$ L_{\mathrm{FQ}}^2 = L_{\mathrm{WF}}^2 + L_{\mathrm{WQ}}^2 - 2L_{\mathrm{WF}}L_{\mathrm{WQ}}\cos\angle\mathrm{FWQ}, \tag{5} $$

where L_{WF} and L_{WQ} represent the lengths of the exoskeleton links WF and WQ, respectively, i.e. $L_{\mathrm{WF}} = L_7$, $L_{\mathrm{WQ}} = L_8$. The length L_{FQ} of edge FQ in triangle FPQ can be expressed as

$$ L_{\mathrm{FQ}}^2 = L_{\mathrm{PF}}^2 + L_{\mathrm{PQ}}^2 - 2L_{\mathrm{PF}}L_{\mathrm{PQ}}\cos\angle\mathrm{FPQ}, \tag{6} $$

where $L_{\mathrm{PF}} = \sqrt{L_{\mathrm{EP}}^2 + L_{\mathrm{EF}}^2} = \sqrt{V^2 + H^2}$, $L_{\mathrm{PQ}} = \sqrt{L_{\mathrm{IP}}^2 + L_{\mathrm{IQ}}^2} = \sqrt{(L_{10} + \delta_x)^2 + (L_9 + \delta_y)^2}$, and $\angle\mathrm{FPQ} = \pi + \theta_P - \arctan((L_4 + L_5)/(L_{11} - q_5)) - \arctan((L_9 + \delta_y)/(L_{10} + \delta_x))$. L_{EP}, L_{EF}, L_{IP}, and L_{IQ} represent the length of links EP, EF, IP, and IQ, respectively.

According to Eqs. (5) and (6), the forward kinematics of the PIP closed-loop kinematic chain can be obtained

$$ \theta_P = \arccos\left(\frac{L_{\mathrm{PF}}^2 + L_{\mathrm{PQ}}^2 - L_7^2 - L_8^2 - 2L_7L_8\cos q_6}{2L_{\mathrm{PF}}L_{\mathrm{PQ}}}\right) + \arctan\left(\frac{L_4 + L_5}{L_{11} - q_5}\right) + \arctan\left(\frac{L_9 + \delta_y}{L_{10} + \delta_x}\right) - \pi. \tag{7} $$

The angle of the PIP f/e motion can be obtained according to Eq. (7), determined by the angle of the exoskeleton joint

q_6. It is worth noting that the displacement of the exoskeleton joint q_5 and the misaligning displacements δ_x, δ_y are regarded as constant or known.

IV. Kineto-Statics Analysis and Optimization

A. Kineto-Statics Modeling

Differentiating (4) yields

$$\dot{\Theta}_P = J(q_P)\dot{q}_P, \tag{8}$$

where $\dot{\Theta}_P$ stands for the velocity vector of the PIP joint, $\dot{q}_P$ represents the velocity vector of the exoskeleton joints, and $J(q_P)$ stands for the Jacobian matrix of the exoskeleton system. The expression of $J(q_P)$ can be calculated by the symbolic computation in MATLAB.

Based on the virtual work principle, there is

$$\tau_{q_P} = J^{\mathrm{T}}(q_P)\tau_{\Theta_P}, \tag{9}$$

where $\tau_{\Theta_P} = [\tau_{\theta_P} \& \tau_{\delta_x} \& \tau_{\delta_y}]^{\mathrm{T}}$ represents the forces /torque of the PIP joint, and τ_{θ_P} is the actuated torque applied in the f/e motion. τ_{δ_x} and τ_{δ_y} are the joint reaction forces applied in the misaligning directions. $\tau_{q_P} = [\tau_{q_{4'}} \& \tau_{q_6} \& \tau_{q_7}]^{\mathrm{T}}$ is the torques of the exoskeleton joints. Eq. (9) can be rewritten as

$$\begin{pmatrix} \tau_{q_{4'}} \\ \tau_{q_6} \\ \tau_{q_7} \end{pmatrix} = \begin{pmatrix} -\tau_{\theta_P} - (G_P + L_7 s_{67})\tau_{\delta_x} + (L_7 c_{67} - J_P)\tau_{\delta_y} \\ \tau_{\theta_P} + G_P \tau_{\delta_x} + J_P \tau_{\delta_y} \\ \tau_{\theta_P} + (G_P + L_8 c_7)\tau_{\delta_x} + (J_P + L_8 s_7)\tau_{\delta_y} \end{pmatrix}, \tag{10}$$

where $G_P = V\sin(q_6 - q_{4'} + q_7 - \pi/2) - H\cos(q_6 - q_{4'} + q_7 - \pi/2) - L_7 s_{67}$, $J_P = -V\cos(q_6 - q_{4'} + q_7 - \pi/2) - H\sin(q_6 - q_{4'} + q_7 - \pi/2) + L_7 c_{67}$.

The driving configuration of the PIP exoskeleton joints has been described in Section II-A. The exoskeleton joints $q_{4'}$, q_7 are passive sliding joints, and their driving torques are zero. The exoskeleton joint q_6 is driven by a Bowden-cable system, and its driving torque is not zero. Therefore, the driving torques of the exoskeleton joints can be expressed as

$$\tau_{q_{4'}} = \tau_{q_7} = 0, \tau_{q_6} \neq 0. \tag{11}$$

Substituting Eq. (11) into Eq. (10) yields

$$\begin{pmatrix} \tau_{\theta_P} \\ \tau_{\delta_x} \\ \tau_{\delta_y} \end{pmatrix} = \begin{pmatrix} U_P \tau_{q_6}/(L_7 L_8 \sin q_6) \\ (L_7 c_{67} + L_8 s_7)\tau_{q_6}/(L_7 L_8 \sin q_6) \\ (-L_7 s_{67} + L_8 c_7)\tau_{q_6}/(L_7 L_8 \sin q_6) \end{pmatrix}, \tag{12}$$

where $U_P = V L_8 \sin(q_{4'} - q_6) + H L_7 \cos q_{4'} + V L_7 \sin q_{4'} + H L_8 \cos(q_{4'} - q_6)$. According to Eq. (12), the force along the phalanx generated by the PIP exoskeleton chain can be obtained, which is τ_{δ_x}.

B. Optimization of Exoskeleton Links Length

A two-level optimization method considering the individual differences in the finger segment sizes is proposed to reduce the force along the phalanx. According to the kineto-statics of the PIP closed-loop kinematic chain, the force along the phalanx is related to the length of the exoskeleton links. The exoskeleton links can be divided into two types: variable-length links and constant-length links. The variable-length links mainly include the links formed by the exoskeleton links and the finger segment, such as links PF and PQ. The length of these links changes with the wearer due to the individual differences in the finger segment size. The length of the link PF is determined by the link EF (related to the height of the proximal phalanx) and the link EP (related to the position of the exoskeleton joint q_5), and the link PQ is determined by the link IP (related to the length of the middle phalanx) and the link IQ (related to the height of the middle phalanx). The constant-length links include the exoskeleton links WF, WQ, and their length is constant.

The force along the phalanx is also related to the angle of the exoskeleton joints q_6, q_7. However, the angles of the exoskeleton joints q_6, q_7 can be expressed by the length of the exoskeleton links. According to the geometric method, the angle of the exoskeleton joint q_7 can be expressed as

$$\begin{aligned} q_7 =& \pi - \arctan\left(\frac{L_{10} + \delta_x}{L_9 + \delta_y}\right) \\ & - \arccos\left(\frac{L_8 + L_7\cos q_6}{\sqrt{L_7^2 + L_8^2 + 2L_7 L_8 \cos q_6}}\right) \\ & - \arccos\left(\frac{L_7^2 + L_8^2 + L_{\mathrm{PQ}}^2 + 2L_7 L_8 \cos q_6 - L_{\mathrm{PF}}^2}{2L_{\mathrm{PQ}}\sqrt{L_7^2 + L_8^2 + 2L_7 L_8 \cos q_6}}\right). \end{aligned} \tag{13}$$

The variation range of the exoskeleton joint q_6 can be expressed by the length of the exoskeleton links. The initial angle of the joint q_6 (the maximum angle) is defined as the angle at the index finger extension, and can be expressed as

$$q_{60} = \arccos\left(\frac{L_{\mathrm{PF}}^2 + L_{\mathrm{PQ}}^2 - L_7^2 - L_8^2 - 2L_{\mathrm{PF}}L_{\mathrm{PQ}}\cos\Upsilon}{2L_7 L_8}\right), \tag{14}$$

where $\Upsilon = \pi - \arctan((L_4 + L_5)/(L_{11} - q_5)) - \arctan((L_9 + \delta_y)/(L_{10} + \delta_x))$. The end angle of the joint q_6 (the minimum angle) is defined as the angle at the collinear position of links PF and PQ, and can be expressed as

$$q_{6\mathrm{e}} = \arccos\left(\frac{L_{\mathrm{PF}}^2 + L_{\mathrm{PQ}}^2 - L_7^2 - L_8^2 + 2L_{\mathrm{PF}}L_{\mathrm{PQ}}}{2L_7 L_8}\right). \tag{15}$$

Therefore, the variation range of the joint q_6 should be

$$q_{6\mathrm{e}} \leqslant q_6 \leqslant q_{60}. \tag{16}$$

It is worth noting that the initial angle of the joint q_6 should be a real number to ensure that the PIP exoskeleton chain can assist the PIP joint to the extended position, and can be expressed as

$$q_{60} \in \mathbb{R}. \tag{17}$$

To make Eq. (15) hold, the triangle WFQ should exist when the links PF, PQ are collinear. Therefore, the PIP closed-loop kenematic chain should meet the following constraint

$$L_7 + L_8 > L_{\mathrm{PF}} + L_{\mathrm{PQ}}. \tag{18}$$

The PIP exoskeleton chain should assist the PIP joint to reach the maximum natural movement position, and this constraint can be expressed as

$$\theta_{\mathrm{Pb}} \leq \arccos\left(\frac{L_{\mathrm{PF}}^2 + L_{\mathrm{PQ}}^2 - L_7^2 - L_8^2 - 2L_7L_8\cos q_{6\mathrm{e}}}{2L_{\mathrm{PF}}L_{\mathrm{PQ}}}\right) - \Upsilon, \tag{19}$$

where θ_{Pb} represents the maximum natural movement angle of the PIP joint. To avoid the huge volume of the PIP exoskeleton chain, the constant-length links need meet the following constraints

$$L_{7\mathrm{b}} \leq L_7 \leq L_{7\mathrm{u}}, L_{8\mathrm{b}} \leq L_8 \leq L_{8\mathrm{u}}, \tag{20}$$

where $L_{7\mathrm{b}}$, $L_{8\mathrm{b}}$ and $L_{7\mathrm{u}}$, $L_{8\mathrm{u}}$ represent the upper and lower bounds of the corresponding constant-length links, respectively. The constraint conditions of the variable-length links can be expressed as

$$\begin{cases} L_{\mathrm{EFb}} \leq L_{\mathrm{EF}} \leq L_{\mathrm{EFu}}, \\ L_{\mathrm{EPb}} \leq L_{\mathrm{EP}} \leq L_{\mathrm{EPu}}, \\ L_{\mathrm{IPb}} \leq L_{\mathrm{IP}} \leq L_{\mathrm{IPu}}, \\ L_{\mathrm{IQb}} \leq L_{\mathrm{IQ}} \leq L_{\mathrm{IQu}}, \end{cases} \tag{21}$$

where L_{EFb}, L_{EPb}, L_{IPb}, L_{IQb} and L_{EFu}, L_{EPu}, L_{IPu}, L_{IQu} represent the upper and lower bounds of the corresponding variable-length links, respectively.

The lower-level optimization problem of the proposed two-level optimization method is to determine the length of the variable-length links and the angle of the exoskeleton joint q_6 with the optimization goal of maximizing the force along the phalanx given the length of the links WF, WQ, and can be expressed as

$$\begin{aligned} &\max \ f_{(L_{\mathrm{EF}}, L_{\mathrm{EP}}, L_{\mathrm{IP}}, L_{\mathrm{IQ}}, q_6)} = \frac{(L_7c_{67} + L_8s_7)\tau_{q_6}}{L_7L_8\sin q_6} \\ &s.t. \ \text{Eqs. (16), (17), (18), (19) and (21).} \end{aligned} \tag{22}$$

The upper-level optimization problem is to determine the length of the constant-length links with the optimization goal of minimizing the force along the phalanx based on the parameters determined by the lower-level optimization problem, and can be expressed as

$$\begin{aligned} &\min \ f_{(L_7, L_8)} = \frac{(L_7c_{67} + L_8s_7)\tau_{q_6}}{L_7L_8\sin q_6} \\ &s.t. \ \text{Eqs. (20) and (22).} \end{aligned} \tag{23}$$

The sizes of the finger segment for six male subjects are measured to determine the range of variation of the variable-length links, as shown in Table II. The subjects' age, weight, and height are 23-32 years old, 54-115 kg, and 170-185 cm, respectively. According to the size requirements of the exoskeleton components, the sizes of the finger segment, and the exoskeleton-phalanx fixture position, the upper and lower bounds of the variable-length links are determined and shown in Table III. Table III also shows the upper and lower bounds of the constant-length links, the maximum natural movement angle of the PIP joint, and the driving torque of the exoskeleton joint q_6. The proposed two-level optimization problem is solved by MATLAB, and optimization results are $L_7 = 51.3$ mm and $L_8 = 35$ mm. Figure 5 shows the three-dimensional model of the index finger exoskeleton before and after optimization.

TABLE II
FINGER SEGMENT SIZE OF DIFFERENT SUBJECTS

	Sub. 1	Sub. 2	Sub. 3	Sub. 4	Sub. 5	Sub. 6
The length of the middle phalanx(mm)	27	30	26	25	23	28
The height of the middle phalanx(mm)	12	16	14	12	11	12
The height of the proximal phalanx(mm)	16	20	17	15	14	17

TABLE III
VALUE OF RELEVANT PARAMETERS OF THE PROPOSED TWO-LEVEL OPTIMIZATION METHOD

θ_{Pb}	90°	$L_{7\mathrm{b}}$	25 mm	$L_{7\mathrm{u}}$	60 mm
τ_{q_6}	0.1 Nm	$L_{8\mathrm{b}}$	25 mm	$L_{8\mathrm{u}}$	35 mm
L_{EFb}	26 mm	L_{EFu}	30 mm	L_{EPb}	9 mm
L_{EPu}	20 mm	L_{IPb}	11 mm	L_{IPu}	15 mm
L_{IQb}	12 mm	L_{IQu}	15 mm		

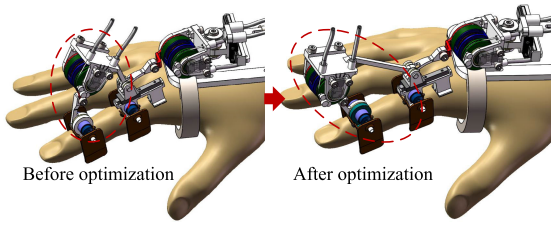

Fig. 5. Comparison of three-dimensional models of the PIP closed-loop kinematic chain before and after optimization.

V. EXPERIMENTAL SETUP

In this section, five experiments have been carried out, and their objectives are 1) to evaluate the convenience of the semi-wrapped fixture, i.e., count the time required for different subjects to don/doff the index finger exoskeleton in different postures; 2) to assess the connection stability of the semi-wrapped fixture, i.e., measure the relative displacement change between the fixture and the phalanx; 3) to assess the comfort of the semi-wrapped fixture, i.e., measure the blood flow change around fixing points and establish the subjects' feelings through a survey questionnaire; 4) to verify the effectiveness of the proposed two-level optimization method; and 5) to evaluate the passive safety of the index finger exoskeleton with the elastomer-based clutched SEA.

A. Convenience of the Semi-Wrapped Fixture

In the first experiment, the convenience of the semi-wrapped fixture is evaluated by comparing the time required to don/doff the index finger exoskeleton with the semi-wrapped fixture or Velcro in different hand postures. Six male subjects who are the same as those in Section IV were recruited. They volunteer to participate in the experiment and sign an informed consent.

This experiment is reviewed and approved by the Institute of Automation Chinese, Academy of Sciences (approval number: IA-202044). Each subject donned/doffed the index finger exoskeleton with the semi-wrapped fixture or the Velcro three times when the hand maintains in an open posture and a fisted posture. The connectors between the exoskeleton and the hand include two Velcros and two semi-wrapped fixtures. The donning processes are as follows

1) Don the Velcros on the palm and wrist;
2) Open the semi-wrapped fixture at the proximal phalanx and don it into the proximal phalanx;
3) Open the semi-wrapped fixture at the middle phalanx and don it into the middle phalanx.

The doffing processes are as follows

1) Open the semi-wrapped fixture at the middle phalanx and doff it from the middle phalanx;
2) Open the semi-wrapped fixture at the proximal phalanx and doff it from the proximal phalanx;
3) Doff the Velcros from the palm and wrist.

The operating processes of the two types of exoskeletons are different due to the different fixtures at the proximal and middle phalanxes, but the operation sequence of the fixtures for the two types of exoskeletons is the same.

B. Connection Stability

The relative sliding between the exoskeleton and the finger segment can make the wearer lose the sense of belonging. In this experiment, the relative displacement between the exoskeleton and the phalanx during the f/e motion is measured to evaluate the connection stability of the semi-wrapped fixture. The exoskeletons with the semi-wrapped fixture or the Velcro were worn on six subjects, respectively. The exoskeleton actively assisted the PIP joint in f/e motion in three hand postures: back of hand up, hand upright, and palm up. Two marker points were placed on the middle phalanx and the fixture, respectively, and their relative displacement change can be recorded by a motion capture system (Prime 13, OptiTrack, USA) equipped with eight high-speed cameras. Meanwhile, to display the relationship between the attaching force and the relative displacement, the relative displacements under different attaching forces are measured when the hand is the hand upright. The experimental steps are the same as before, except for changing the attaching force. The attaching force can ensure stable connection between the exoskeleton and the index finger.

C. Comfort of the Semi-Wrapped Fixture

According to ref. [22], the comfort of the proposed semi-wrapped fixture can be evaluated by blood flow around fixing points. The blood flow contraction is inferred based on the temperature depression of a fixed point since it is difficult to directly measure the blood flow change. Two temperature sensors (DS18B20+) were placed on the finger root (between the MCP joint and PIP joint) and fingertip (between the fingertip and DIP joint) of the index finger for six recruited subjects to measure the temperature of the user's skin surface. The index finger exoskeleton was donned on the subjects.

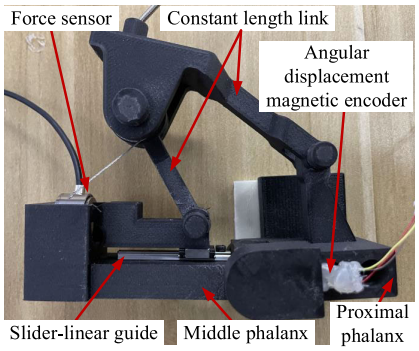

Fig. 6. An experimental platform for measuring the forces along the phalanx generated by the PIP exoskeleton chain.

After stabilizing the skin surface's temperature, the index finger exoskeleton assisted the PIP joint in the f/e motion, and the temperature of the subject's skin surface was recorded every 5 seconds for one hour. The room temperature during this measurement was approximately 26°C.

D. Evaluation of the Force Along the Phalanx

The force along the phalanx generated by the index finger exoskeleton is measured to verify the effectiveness of the two-level optimization method. As shown in Fig. 6, an experimental platform with the same kineto-statics relationship as the PIP closed-loop kinematic chain was designed and fabricated to measure the force along the phalanx. The experimental platform is mainly composed of the proximal phalanx, the middle phalanx, a slider-linear guide, an angular displacement magnetic encoder, a force sensor, etc. The lengths of the variable-length links are constant values here. The angular displacement magnetic encoder was placed on the PIP joint to measure its flexion angle. The slider-linear guide was placed between the middle phalanx and the constant-length link WQ to make the exoskeleton and phalanx slide relatively. The force sensor (DYZ-100, Freud) was placed on the front of the slide-linear guide to measure the force along the phalanx. No force sensor was placed on the back of the slide-linear guide since the force can be ignored during the flexion motion. The force along the phalanx measured by the force sensor and the joint angle measured by the angular displacement magnetic encoder were recorded by a DSpace. For comparison, the PIP closed-loop kinematic chain before optimization can be built by replacing the constant-length links, and the force along the phalanx was measured.

E. Passive Safety

In this experiment, the passive safety of the proposed index finger exoskeleton with the elastomer-based clutched SEA is evaluated by measuring the interaction force between the exoskeleton and the index finger. An experimental platform, including the index finger exoskeleton with the elastomer-based clutched SEA, was built as shown in Fig. 7. The index finger exoskeleton was worn on the index finger. A force sensor (the same as the one in the previous experiment) was placed between the exoskeleton and the phalanx to measure the interaction force. The input end of

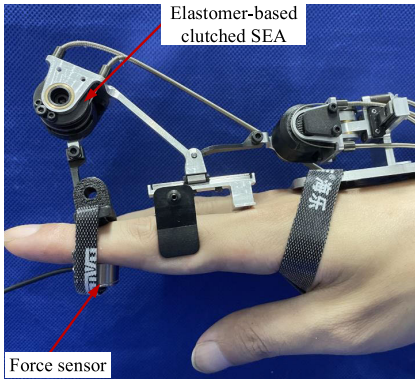

Fig. 7. An experimental platform for measuring the interaction forces between the index finger exoskeleton with the elastomer-based clutched SEA and the phalanx.

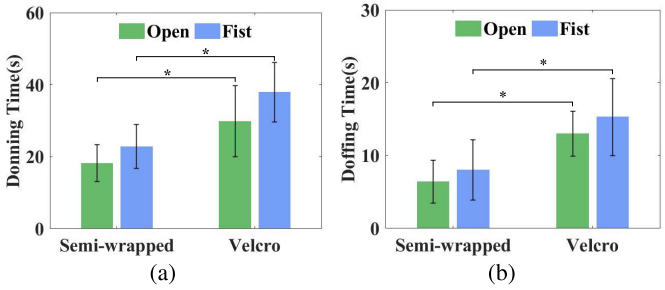

Fig. 8. The mean donning/doffing time and variation range for six subjects in different postures. (a) Donning, (b) Doffing.

the SEA was locked by a Bowden-cable system. The PIP joint actively performed rapid flexion movements to simulate sudden movement caused by muscle spasms in stroke patients. In addition, the index finger exoskeleton without the elastomer-based clutched SEA was also worn on the index finger, and the interaction force was measured in the same way. To explore the relationship between the passive safety of the index finger exoskeleton and the maximum transmission torque of the elastomer-based clutched SEA, the deformation of the Belleville spring in the elastomer-based clutched SEA was adjusted, and the interaction force between the index finger exoskeleton and the phalanx was measured in the same way.

VI. Results and Discussions

A. Convenience of the Semi-Wrapped Fixture

Figure 8 shows the mean donning/doffing time and variation range for six subjects in different hand postures. The analysis of variance (ANOVA) reveals a significant difference in donning/doffing time between the different fixtures (ANOVA, $^*P < 0.001$). The semi-wrapped fixture requires less time for donning/doffing compared to the Velcro. Therefore, the semi-wrapped fixture can improve the convenience of donning/doffing.

B. Connection Stability

The influence of hand posture is researched. Figure 9 shows the mean values and variation ranges of the relative displacement for six subjects in three hand postures. The ANOVA

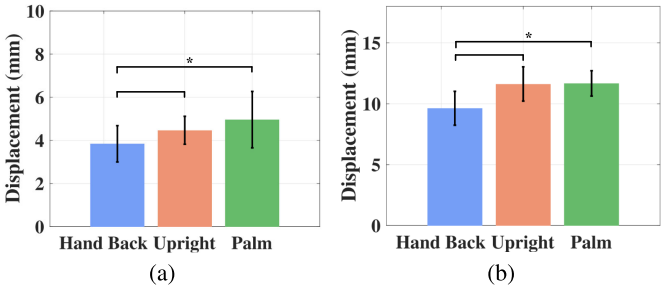

Fig. 9. The mean values and variation ranges of the relative displacement for six subjects in three hand postures. (a) Semi-wrapped fixture; (b) Velcro.

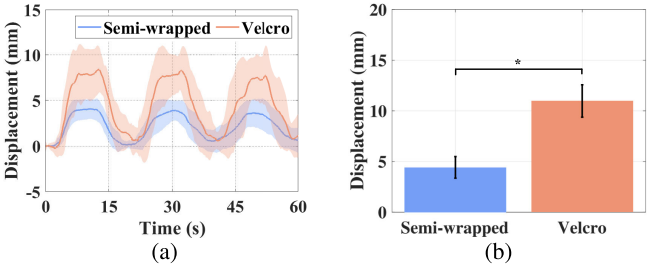

Fig. 10. The curves, mean values, and variation ranges of the sum of the relative displacement with different wearing structures of six subjects. (a) Curves; (b) Mean value and variation range.

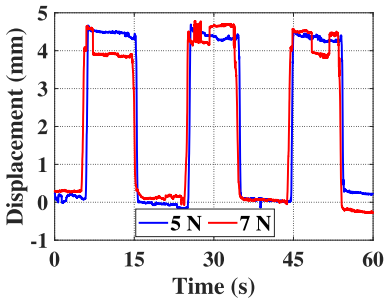

Fig. 11. The relative displacement under the different attaching forces: 5 N and 7 N.

is used to show the difference between different data sets. There are significant differences in the relative displacement between the back of hand up and the palm up (ANOVA, $^*P < 0.001$), which can be caused by the gravity of index finger exoskeleton.

Meanwhile, we combine the relative displacement data sets in different hand postures and compare the influence of different wearing structures. Figure 10 shows the mean values and variation ranges of the combined relative displacement data sets for six subjects. The shaded region in Fig. 10(a) represents the mean $\pm$ one standard deviation. In Fig. 10(b), it is obvious that the relative displacement of the semi-wrapped fixture is less than that of the Velcro (ANOVA, $^*P < 0.001$). Compared with the Velcro, the average value of the maximum relative displacement is reduced by 59.7%. Therefore, the proposed semi-wrapped fixture can improve the connection stability between the exoskeleton and the phalanx.

Figure 11 shows the relative displacement under the different attaching forces: 5 N and 7 N. The relative displacements

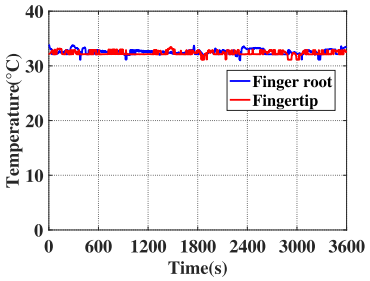

Fig. 12. The transition of skin surface temperature for a subject.

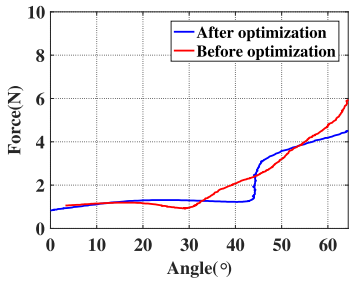

Fig. 13. The force along the phalanx generated by the PIP exoskeleton chain before and after optimization.

are basically consistent. The result indicates that the relative displacements can be caused by skin deformation when sufficient attaching force is provided.

C. Comfort of the Semi-Wrapped Fixture

Figure 12 shows the transition of skin surface temperature for a subject. The skin temperatures of the index finger remain basically constant. Therefore, the proposed semi-wrapped fixture does not block blood flow in the f/e motion. Meanwhile, each subject filled out a survey questionnaire on the comfort of the fixture after training. All subjects strongly agree or agree that the semi-wrapped fixture is comfortable and easy to don/doff. In summary, the proposed semi-wrapped fixture can ensure comfort.

D. Evaluation of the Force Along the Phalanx

Figure 13 shows the forces along the phalanx generated by the PIP exoskeleton chain before and after optimization. The maximum values of the forces along the phalanx generated by the PIP exoskeleton chain before and after optimization are 5.92 N and 4.52 N, respectively. Compared with the PIP exoskeleton chain before optimization, the maximum force generated by the PIP exoskeleton chain after optimization can be reduced by 23.65%. Therefore, the proposed two-level optimization method for the PIP closed-loop kinematic chain is effective. The PIP closed-loop kinematic chain after optimization can reduce the maximum force along the phalanx and avoid damage by the exoskeleton to the finger skin. It is worth noting that the force along the phalanx increases with the increase of the flexion angle of the PIP joint.

E. Passive Safety

Figure 14 shows the interaction force between the index finger exoskeleton and finger phalanx. Compared with the

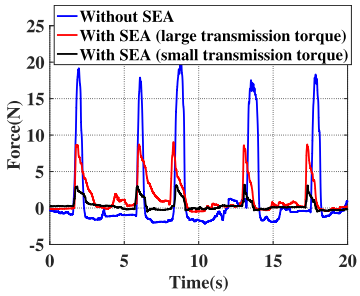

Fig. 14. The interaction forces between the index finger exoskeleton with and without the elastomer-based clutched SEA and the phalanx.

exoskeleton without the SEA, the exoskeleton with the elastomer-based clutched SEA can reduce the interaction force and improve passive safety. The experimental results also show that the smaller the maximum transmission torque of the index finger exoskeleton, the smaller the interaction force between the index finger exoskeleton and the phalanx. Therefore, reducing the maximum transmission torque of the SEA can improve the passive safety of the index finger exoskeleton.

F. Discussions

This paper proposes an index finger exoskeleton with semi-wrapped fixtures and elastomer-based clutched SEAs to improve the convenience of donning/doffing, connection stability, comfort, and passive safety. The semi-wrapped fixture was developed to replace the traditional fixture-the Velcro [17], [18]. Statistical analysis results indicate that the donning/doffing time of the semi-wrapped fixture are less than that of the Velcro. The average value of the maximum relative displacement for the semi-wrapped fixture is reduced by 59.7% compared to the Velcro. Moreover, the consistent skin temperature around the fixture and the satisfaction survey of the subjects after long-term training indicate the comfort of the semi-wrapped fixture. The elastomer-based clutched SEA can limit the maximum interaction force between the exoskeleton and the index finger, and improve passive safety, as shown in Fig. 14.

The interaction force between the exoskeleton and the index finger can be divided into the force along the phalanx and the force perpendicular to the phalanx. The force along the phalanx only loads the joint without resulting in any joint movement. To reduce the force along the phalanx, the two-level optimization method for the PIP closed-loop kinematic chain was proposed. The exoskeleton after optimization can reduce the maximum force along the phalanx by 23.65% compared to the exoskeleton before optimization. It is worth noting that the index finger exoskeleton was optimized based on the finger size of the six recruited subjects in this paper. Therefore, the proposed exoskeleton is suitable for the subjects with a middle phalanx length and height between 23-30 mm and 11-16 mm, respectively. A more universal index finger exoskeleton can be designed by expanding the range of changes in finger size.

However, the experimental studies have several limitations that need to be addressed in future studies. First, the experimental results show that the relative displacements are consistent under different attaching forces. The minimum attaching

force required for different rehabilitation training or grasping tasks needs to be further determined to avoid discomfort caused by excessive attaching force. Second, the effectiveness of the two-level optimization method has been verified based on the size of a subject's index finger. We need to measure the force along the phalanx generated by the optimized exoskeleton on different subjects to explore the performance differences of the optimization method on different subjects. Finally, the elastomer-based clutched SEA has been applied in the exoskeleton, enabling it to achieve force control. The force control performance of the proposed index finger exoskeleton needs to be studied further.

VII. Conclusion

In this paper, an index finger exoskeleton with semi-wrapped fixtures and elastomer-based clutched SEAs was proposed. The semi-wrapped fixture was developed to improve the convenience of donning/doffing and connection stability. Second, the kinematic compatibility of the PIP exoskeleton chain was analyzed, and its forward kinematics was established based on the geometric method. Third, the kineto-statics of the PIP exoskeleton chain was studied, and a two-level optimization method was proposed to reduce the force along the phalanx. Finally, the experiments on the performance of the index finger exoskeleton were conducted. Compared with the Velcro, the average value of the maximum relative displacement is reduced by 59.7%. Compared with the exoskeleton before optimization, the maximum force along the phalanx generated by the exoskeleton after optimization is reduced by 23.65%. The experimental results show that the proposed exoskeleton can improve the convenience of donning/doffing, connection stability, comfort, and passive safety.

References

[1] A. Alizadeh, S. M. Dyck, and S. Karimi-Abdolrezaee, "Traumatic spinal cord injury: An overview of pathophysiology, models and acute injury mechanisms," *Frontiers Neurol.*, vol. 10, p. 282, Mar. 2019.

[2] A. Todhunter-Brown et al., "Physical rehabilitation approaches for the recovery of function and mobility following stroke," *Cochrane Database Systematic Rev.*, vol. 2023, no. 4, Apr. 2014, Art. no. CD001920.

[3] X. L. Hu, K. Y. Tong, X. J. Wei, W. Rong, E. A. Susanto, and S. K. Ho, "Coordinated upper limb training assisted with an electromyography (EMG)-driven hand robot after stroke," in *Proc. 35th Annu. Int. Conf. IEEE Eng. Med. Biol. Soc. (EMBC)*, Jul. 2013, pp. 5903–5906.

[4] C. D. Takahashi, L. Der-Yeghiaian, V. Le, R. R. Motiwala, and S. C. Cramer, "Robot-based hand motor therapy after stroke," *Brain*, vol. 131, no. 2, pp. 425–437, Feb. 2008.

[5] W. Chen et al., "Soft exoskeleton with fully actuated thumb movements for grasping assistance," *IEEE Trans. Robot.*, vol. 38, no. 4, pp. 2194–2207, Aug. 2022.

[6] H. Zhao, J. Jalving, R. Huang, R. Knepper, A. Ruina, and R. Shepherd, "A helping hand: Soft orthosis with integrated optical strain sensors and EMG control," *IEEE Robot. Autom. Mag.*, vol. 23, no. 3, pp. 55–64, Sep. 2016.

[7] H. Li, L. Cheng, Z. Li, and W. Xue, "Active disturbance rejection control for a fluid-driven hand rehabilitation device," *IEEE/ASME Trans. Mechatronics*, vol. 26, no. 2, pp. 841–853, Apr. 2021.

[8] *Sinfonia*. Accessed: Dec. 2022. [Online]. Available: https://www.gloreha.com/sinfonia/

[9] M. Cempini, M. Cortese, and N. Vitiello, "A powered finger–thumb wearable hand exoskeleton with self-aligning joint axes," *IEEE/ASME Trans. Mechatronics*, vol. 20, no. 2, pp. 705–716, Apr. 2015.

[10] M. Dragusanu, M. Z. Iqbal, T. L. Baldi, D. Prattichizzo, and M. Malvezzi, "Design, development, and control of a hand/wrist exoskeleton for rehabilitation and training," *IEEE Trans. Robot.*, vol. 38, no. 3, pp. 1472–1488, Jun. 2022.

[11] D. Wang, Q. Meng, Q. Meng, X. Li, and H. Yu, "Design and development of a portable exoskeleton for hand rehabilitation," *IEEE Trans. Neural Syst. Rehabil. Eng.*, vol. 26, no. 12, pp. 2376–2386, Dec. 2018.

[12] R. Casas, M. Sandison, T. Chen, and P. S. Lum, "Clinical test of a wearable, high DOF, spring powered hand exoskeleton (HandSOME II)," *IEEE Trans. Neural Syst. Rehabil. Eng.*, vol. 29, pp. 1877–1885, 2021.

[13] R. A. Bos, K. Nizamis, B. F. J. M. Koopman, J. L. Herder, M. Sartori, and D. H. Plettenburg, "A case study with symbihand: An sEMG-controlled electrohydraulic hand orthosis for individuals with Duchenne muscular dystrophy," *IEEE Trans. Neural Syst. Rehabil. Eng.*, vol. 28, no. 1, pp. 258–266, Jan. 2020.

[14] H. Li, L. Cheng, N. Sun, and R. Cao, "Design and control of an underactuated finger exoskeleton for assisting activities of daily living," *IEEE/ASME Trans. Mechatronics*, vol. 27, no. 5, pp. 2699–2709, Oct. 2022.

[15] M. Cempini et al., "Kinematics and design of a portable and wearable exoskeleton for hand rehabilitation," in *Proc. IEEE 13th Int. Conf. Rehabil. Robot. (ICORR)*, Seattle, WA, USA, Jun. 2013, pp. 1–6.

[16] N. Sun, G. Li, and L. Cheng, "Design and validation of a self-aligning index finger exoskeleton for post-stroke rehabilitation," *IEEE Trans. Neural Syst. Rehabil. Eng.*, vol. 29, pp. 1513–1523, 2021.

[17] K. Ma, Z. Jiang, S. Gao, X. Cao, and F. Xu, "Design and analysis of fiber-reinforced soft actuators for wearable hand rehabilitation device," *IEEE Robot. Autom. Lett.*, vol. 7, no. 3, pp. 6115–6122, Jul. 2022.

[18] E. Capotorti et al., "A novel torque-controlled hand exoskeleton to decode hand movements combining SEMG and fingers kinematics: A feasibility study," *IEEE Robot. Autom. Lett.*, vol. 7, no. 1, pp. 239–246, Jan. 2022.

[19] J. A. Díez, A. Blanco, J. M. Catalán, F. J. Badesa, L. D. Lledó, and N. García-Aracil, "Hand exoskeleton for rehabilitation therapies with integrated optical force sensor," *Adv. Mech. Eng.*, vol. 10, no. 2, pp. 1–11, 2018.

[20] V. Moreno-SanJuan, A. Cisnal, J.-C. Fraile, J. Pérez-Turiel, and E. De-La-Fuente, "Design and characterization of a lightweight underactuated RACA hand exoskeleton for neurorehabilitation," *Robot. Auto. Syst.*, vol. 143, Sep. 2021, Art. no. 103828.

[21] J. Vertongen and D. Kamper, "Design of a 3D printed hybrid mechanical structure for a hand exoskeleton," *Current Directions Biomed. Eng.*, vol. 6, no. 2, Oct. 2020, Art. no. 20202003.

[22] Y. Hasegawa and T. Suzuki, "Thin and active fixture to hold finger for easy attachment and comfort of grasping support exoskeleton," in *Proc. IEEE Int. Conf. Robot. Autom. (ICRA)*, Seattle, WA, USA, May 2015, pp. 4973–4978.

[23] S. P. Buerger and N. Hogan, "Complementary stability and loop shaping for improved human–robot interaction," *IEEE Trans. Robot.*, vol. 23, no. 2, pp. 232–244, Apr. 2007.

[24] D. Marconi, A. Baldoni, Z. McKinney, M. Cempini, S. Crea, and N. Vitiello, "A novel hand exoskeleton with series elastic actuation for modulated torque transfer," *Mechatronics*, vol. 61, pp. 69–82, Aug. 2019.

[25] Y. Guo, W. Xu, S. Pradhan, C. Bravo, and P. Ben-Tzvi, "Data driven calibration and control of compact lightweight series elastic actuators for robotic exoskeleton gloves," *IEEE Sensors J.*, vol. 21, no. 19, pp. 21120–21130, Oct. 2021.

[26] P. Agarwal and A. D. Deshpande, "Series elastic actuators for small-scale robotic applications," *J. Mech. Robot.*, vol. 9, no. 3, Jun. 2017, Art. no. 031016.

[27] M. Bianchi et al., "Design of a series elastic transmission for hand exoskeletons," *Mechatronics*, vol. 51, pp. 8–18, May 2018.

[28] N. Sun, L. Cheng, and X. Xia, "Design and hysteresis modeling of a miniaturized elastomer-based clutched torque sensor," *IEEE Trans. Instrum. Meas.*, vol. 71, pp. 1–9, 2022.

[29] G. Li, L. Cheng, Z. Gao, X. Xia, and J. Jiang, "Development of an untethered adaptive thumb exoskeleton for delicate rehabilitation assistance," *IEEE Trans. Robot.*, vol. 38, no. 6, pp. 3514–3529, Dec. 2022.